Investigations of Singlet and Triplet Diffusion in Thermally-Activated Delayed-Fluorescence Emitters: Implications for Hyperfluorescence

Marius Jakoby, Bryce S. Richards, Uli Lemmer, and Ian A. Howard*
Institute of Microstructure Technology, Karlsruhe Institute of Technology, Hermann-von-Helmholtz-Platz 1, D-76344 Eggenstein-Leopoldshafen, Germany.
(Dated: June 25, 2019)

The exciton transport is particularly intriguing in molecules with intramolecular charge-transfer states that show thermally-activated delayed fluorescence (such as 4CzBN), as in these cases it is defined by multiple cycles through singlet and triplet spin-configurations that have significantly different transport properties. Thus, the overall exciton transport has contributions from both the singlet and triplet exciton diffusion. Herein, we investigate with Monte Carlo simulations how the singlet and triplet diffusion lengths can be experimentally established for this unique class of molecules. We then consider how the efficiency of diffusive transfer to a fluorescence acceptor (hyperfluorescence) is affected by modifications of the triplet and singlet transfer rates. Importantly, we theoretically predict that high efficiency hyperfluorescence can be achieved in an active layer by ensuring that triplet transport between TADF molecules is poor.

I. INTRODUCTION

In an organic light-emitting diode (OLED), three out of four charge recombination events lead to triplet excitons[1]. Therefore, to be efficient, OLEDs must integrate these triplet excitons into the light emitting process. One strategy is the use of phosphorescent dopants. These, often utilizing heavy metal atoms (mainly iridium metal complexes), enhance the spin-orbit coupling and thereby the intermixing of singlet and triplet states. In turn this increases the quantum yield of radiative intersystem crossing (ISC). Phosphorescent OLEDs can reach internal quantum efficiencies of close to 100 % *via* emission from the triplet state (since the electrically generated singlet states transition quickly into the lower-lying triplet state as a consequence of high ISC rates)[2,3]. However, the reliance on phosphorescence-based emission for light emitting devices has some undesirable aspects. Beyond the commercial challenge of the relatively high cost of the iridium complexes, technical challenges include the insufficient stability of blue-emitting phosphorescent OLEDs for commercial applications, and the relatively broad emission spectra of phosphorescent emitters[4–6].

A second strategy to harvest triplet excitons, developed extensively in the past few years, is to employ molecules in which the energetic splitting between the singlet and triplet levels is sufficiently small to allow efficient thermal transfer of population from the triplet to the singlet state at room temperature[7–9]. The design paradigm for creating molecules with such small singlet-triplet splitting that maintain good oscillator strengths for emission is to synthesize compact molecules that nonetheless have negligible HOMO-LUMO overlap[10–12]. It remains to be seen whether this interesting class of thermally-activated delayed fluorescence (TADF) molecules will manage to displace phosphorescent emitters in OLED stacks, but the concept of 'hyperfluorescence' may be critical in helping them to do so.

Hyperfluorescence entails the transfer of energy from the TADF molecules to the singlet state of a fluorescent emitter dopant. By reducing both the emission bandwidth, and the excited-state lifetime, this strategy should increase the value and stability of TADF molecules in OLED applications[13]. We note that an analogous approach has also been considered for phosphorescent dopants[14]. However, the goal of achieving efficient hyperfluorescence in active layers including TADF molecules opens interesting novel questions with regard to the transport of excited-states between TADF molecules. Excitons created on TADF dopants must diffuse between TADF molecules until they can be transferred to a fluorescent emitter. The diffusion between TADF molecules may take place when the excited-state is in the singlet or in the triplet spin configuration. The transfer rates will vary significantly based on the current spin configuration. Also, the last transfer to the fluorescent molecule could occur from the singlet state (wanted) or triplet state (unwanted). These excitation, transport, and recombination pathways are schematically illustrated in Fig. 1.

In this contribution, we first develop a Monte Carlo (MC) simulation to study how the singlet and triplet diffusion lengths for TADF molecules can be obtained from experimental data. Secondly, we show that singlet and triplet diffusion lengths can be determined from Stern-Volmer type analysis of the prompt and delayed fluorescence quenching, or from an analytic fit we develop of the total fluorescence quenching (if the prompt and delayed lifetimes of the unquenched molecule are known). This moves beyond the excellent initial work of Menke *et al.* who needed to use a calculated singlet diffusion length in order to separate the measured total diffusion length into singlet and triplet contributions[15]. Finally, we consider how the efficiency of hyperfluorescence is affected by various possible combinations of singlet and triplet transfer rates. We find that poor triplet transport between the TADF molecules can ensure efficient hyperfluorescence, even when the fluorescent dopant is not protected by a blocking-sheath. Given the orthogo-

nal nature of the HOMO and LUMO in TADF molecules it may well be possible to purposefully suppress triplet transport by designing structures to exclude the concurrent HOMO-HOMO and LUMO-LUMO overlap between adjacent molecules needed for the dual-electron-exchange-based triplet transfer. As a further remark, we want to emphasize that we limit our study on TADF molecules with intramolecular charge-transfer states such as 4CzBN. Also, no higher order effects like triplet-triplet annihilation are considered in this publication and therefore the suggested experiments have to be conducted at low enough excitation densities to prevent second-order effects.

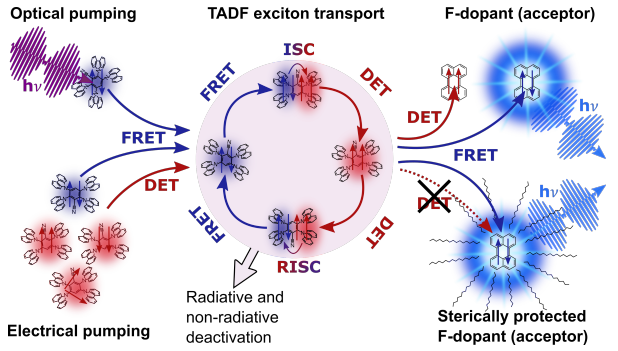

FIG. 1. Schematic of exciton motion in a TADF based device. Singlets can migrate by Förster resonant energy transfer (FRET) between adjacent TADF molecules and fluorescent dopants (F-dopants), or undergo intersystem crossing (ISC) to a triplet state. Triplets either migrate by Dexter type energy transfer (DET) between neighboring TADF molecules and F-dopants (loss mechanism) or reverse intersystem cross into a singlet state (RISC).

II. SIMULATION TECHNIQUE

Monte Carlo simulations are well suited to investigating transport phenomena in organic semiconductors[16–18]. We simulated hyperfluorescent systems comprised of TADF sensitizers and fluorescent emitters embedded in an inert host matrix. All molecules are placed on a square lattice with constant separation (for the purposes of this study we choose the separation to be 1 nm, but this is not important as the simulation is scalable). We consider that all molecules of the same type are iso energetic. Hopping rates ξ_{ij} are determined using the Förster and Dexter theory of energy transfer. For singlets moving by Förster resonant energy transfer, the rate ξ_{ij} is given by[19]:

$$\xi_{ij} = k_\mathrm{s} \left(\frac{R_{ij}^0}{d_{ij}} \right)^6 , \tag{1}$$

where k_s is the singlet decay rate, R_{ij}^0 the FRET radius and d_{ij} the separation of the two sites involved in the transfer. The FRET radius can take on two values, depending if the transfer involves two TADF molecules or a TADF and an emitter molecule. For triplet and singlet Dexter-type transport, the transfer rates are calculated using the following equation[20]:

$$\xi_{ij} = K J_\mathrm{D} e^{-\frac{2 d_{ij}}{L}} , \tag{2}$$

where L stands for the effective Bohr radius, J_D is the normalized spectral overlap integral, while K is related to the specific orbital interaction.

An excited state is introduced to the matrix and two random numbers are generated to determine its lifetime (based on the exponential lifetime distribution of the state), and how the excited state will decay (i.e. radiative, non-radiative, ISC, or reverse-intersystem crossing (RISC)). The excited-state then propagates through the matrix by hopping, as described below, until its lifetime is reached. If ISC occurs, new random numbers are selected for the decay mechanism and a lifetime of the new spin state. This continues until the excited state decays. At this time the root mean square displacement of the excited state is recorded and added to a histogram. An event is also recorded at this time in a histogram tracking the number of excited-states that have left the system. Also, if the exciton undergoes radiative recombination, a counter for emitted photons is increased by one. By dividing this last counter by the total number of excited-states (sequentially) introduced to the system, the PLQY can be found. Further histograms are also kept for generality, but not necessary for the following application.

The MC step of our simulation is based on the Direct Method of Gillespie[21], shortly discussed in the following. In this method, first a list of all possible hopping rates ξ_{ij} from the current position i to neighboring TADF and acceptor molecules j is determined. Second, two random numbers X_1 and X_2 are drawn from the uniform distribution in the unit interval and a hop with rate ξ_{ik} is selected by the first random number:

$$\sum_{j=1}^{k-1} \xi_{ij} < X_1 \sum_{j=1}^{j_\mathrm{max}} \xi_{ij} \leq \sum_{j=1}^{k} \xi_{ij} . \tag{3}$$

The second random number is used to calculate the waiting time Δt for this hop, using inverse transform sampling:

$$\Delta t = -\frac{\ln(X_2)}{\sum_{i=1}^{j_\mathrm{max}} \xi_{ij}} . \tag{4}$$

In order to decrease the runtime of the simulation, the search for new hops to TADF molecules is stopped once the rate of the last added hop is less than 1% of the first (fastest) rate. The simulation is written to include additionally to the matrix and TADF molecules three types of acceptors: 1) charge transfer quenchers to which the singlet and triplet states hop with the same rate

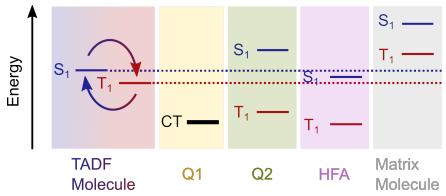

FIG. 2. Schematic of the alignment of energy levels of the different molecules used in the simulations. The different depicted energy levels are the first excited singlet (S_1), the first triplet (T_1) and a charge transfer state (CT). The charge transfer quencher (Q1) and the triplet only quencher (Q2) are used in the simulations of Stern-Volmer analyses of Section III A and III B, respectively, while the hyperfluorescence acceptor (HFA) is used for the simulation of a hyperfluorescent system in Section IV.

(one exponentially-decaying with distance). 2) triplet-only quenchers with the first excited singlet state above and the triplet state below those of the TADF molecules. Here, only the triplet state can transfer (via a Dexter mechanism). 3) fluorescence acceptors to which singlet excitons can transfer by FRET and triplet states by Dexter transfer. An overview of the different types of molecules used in the simulation is given by Fig. 2, where the relative positions of the first excited states with reference to the TADF molecule are schematically shown. During a simulation, a list of all acceptor positions is kept, and hopping rates to acceptors are also added until the last rate added is less than 1 % of the fastest rate to a TADF dopant. Rates to TADF dopants are searched by scanning over adjacent lattice positions, while FRET rates to emitter molecules are found by a loop over all by distance sorted acceptor positions.

In order to verify the results of the MC simulation, we have compared it with analytic solutions for two specific cases of the reaction-diffusion equation of the system under study. Full details regarding the analytic solutions to these two cases and their agreement with the MC findings are shown in the supporting information[22]. Interestingly, one specific case that we examine is the steady state solution for the problem of constant generation of singlet excitons at the origin as the boundary condition. Experimentally, this would be equivalent to generating excitons with an infinitely tightly-focused continuous-wave optical source and observing the concentration of the excited states as a function of radius from this origin. The uniqueness of the diffusion in TADF films, wherein transport happens both in the singlet and triplet state, is clearly visible in this test case. The excited-state profiles cannot be described by the diffusion of a single state with an 'average' diffusion constant. To correctly describe such a system, a full consideration of both singlet and triplet states with their associated diffusion constants is necessary.

In the following, all decay rates (k_r^s, k_nr^s, k_ISC, k_r^t, k_nr^t and k_RISC) have been selected in accordance to one of the benchmark TADF molecules 2,3,5,6-tetra(9H-carbazol-9-yl)benzonitrile (4CzBN)[7]. We will now use the MC approach to simulate experimentally-observable data and ascertain whether, and in what cases, singlet and triplet diffusion lengths can be independently established from experimental data.

III. DETERMINATION OF SINGLET AND TRIPLET DIFFUSION LENGTHS

Common approaches to extract exciton diffusion lengths in organic semiconductors include: 1) luminescence quenching experiments using either molecular mixtures or bilayer structures[23–28]. 2) observing the rates of second-order exciton-exciton annihilation processes[29,30]. We will consider the first approach herein. The only direct study of exciton transport study by TADF molecules of which we are aware was conducted by Menke and Holmes using the approach of thickness-dependent PL quenching experiments[15]. These experiments allowed the total diffusion length to be extracted from fitting the dependence of the PL quenching on the thickness of a TADF film on top of a quenching surface. The square of the total diffusion length (like that experimentally determined by Menke *et al.*) contains contributions of the individual diffusion lengths of the singlets and the triplets:

$$L = \sqrt{6n\left(\frac{D_\mathrm{s}}{k_\mathrm{s}} + \frac{D_\mathrm{t}}{k_\mathrm{t}}\phi_\mathrm{ISC}\right)}, \tag{5}$$

where $n = \sum_{m=0}^{\infty}(\phi_\mathrm{ISC}\phi_\mathrm{RISC})^m$ is the average number of passes through the singlet state and ϕ_RISC and ϕ_ISC the RISC and ISC crossing efficiency, respectively. With two unknowns and only one equation, Menke *et al.* separated the measured total diffusion length into the singlet and triplet diffusion lengths by using Förster theory to provide calculated estimate of the singlet diffusion length.

Herein, we consider whether time-resolved measurements of the PL quenching using the Stern-Volmer approach of molecularly-dispersed quenchers are sufficient to experimentally determine both the singlet and triplet diffusion lengths independently. For this, we performed simulations in which A) charge-transfer quenchers and B) triplet quenchers were randomly distributed with varying concentrations ranging from 0 % to 5 % relative to the TADF molecules. 80 % of the lattice positions were selected to be matrix molecules, as this is a typical TADF doping concentration in the host for OLED devices. The singlet and triplet decay, as well as ISC rates were set to the values of the TADF molecule 4CzBN. The transfer rate to an adjacent acceptor was chosen to be one order of magnitude higher than the rate of singlet transfer to an adjacent TADF molecule. We choose reasonable nearest neighbor singlet transfer rates of $40.8\,\mathrm{ns}^{-1}$ corresponding to a Förster radius of 2 nm[31]. In the below simulations, the diffusion length of the singlets can be established by tracking the root mean square displacement of the singlet states within their lifetime, averaging over

5×10^4 simulated excitons these parameters lead to the singlet diffusion length of 18.1 nm. We note that this is the total singlet diffusion length, including the motion of singlets regenerated from the triplet state. The singlet diffusion length in the initial prompt lifetime only is 7.4 nm, comparable to standard singlet diffusion lengths in organic materials[32,33]. In all simulations, these singlet transfer kinetics (and hence the singlet diffusion length) is held constant. We vary the triplet transfer rates in a reasonable range from 0 ns^{-1} to 2.1 ns^{-1}, consistent with typical triplet transfer rates found in the literature[15]. Again, 5×10^4 simulated excitons for each rate establish that triplet diffusion lengths varies from 0 nm to 50.4 nm (established by tracking the root mean square displacement made while in the triplet state). We now consider whether these known diffusion lengths can be accurately established from experimentally accessible data.

We recreate the experimentally accessible quantities of the prompt emission, delayed emission, and the total emission. These quantities can be measured easily using appropriate gate delays and width on an ICCD, or steady-state measurements with and without a triplet quencher (like oxygen). In the following, we use the MC simulation to track the number of photons emitted (normalized to the total number of injected exciton iterations) in the prompt emission (i.e. from the singlet state before ISC) and the delayed emission (i.e. from a recreated singlet state that has been at least once in the triplet manifold) as a function of the quencher concentration. P_0 and D_0 will refer to the unquenched values for the prompt and delayed emission, whereas P and D are the prompt and delayed emission at a given quencher concentration.

A. Stern-Volmer analysis based on charge transfer quenchers

In this subsection, we establish to which extent a charge transfer acceptor (compare Q1 in Fig. 2), quenching both singlets and triplet excitons with similar rates, can be used to determine both diffusion lengths. For this type of quencher a Stern-Volmer plot for the prompt quenching is directly accessible from the 'raw' data. We also show how a Stern-Volmer plot for exclusively the delayed emission can be obtained once the prompt quenching curve is known. We then consider when and how the singlet and triplet diffusion lengths can be independently ascertained from the analysis of these Stern-Volmer plots. The most intuitive experiment to extract the singlet diffusion length is to analyse the prompt Stern-Volmer plot. The quenching of the prompt emission is exclusively due to singlet motions, so it should be possible to extract the singlet diffusion length from the prompt Stern-Volmer plot in exactly the normal fashion. The triplet diffusion length should have no effect on the prompt quenching. In Fig. 3 the simulated Stern-Volmer plot for the prompt PL is shown, with the different symbols representing quencher concentration simulation runs for the various triplet diffusion lengths. As expected all data points lie on a straight line in accordance with the Stern-Volmer equation:

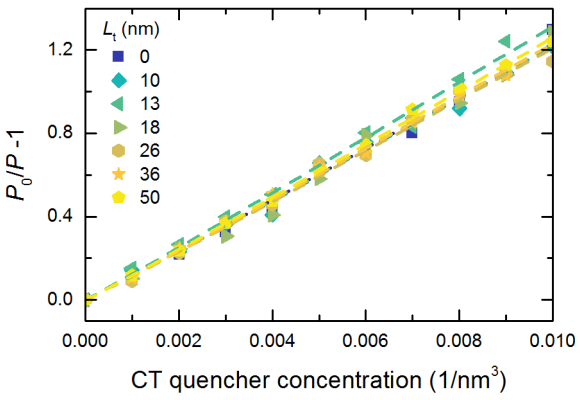

FIG. 3. Stern-Volmer plot based on the prompt PL. Here P_0 is the unquenched and P the quenched PL intensity.

$$K_P[Q] = \frac{P_0}{P} - 1. \tag{6}$$

Here, $[Q]$ is the quencher concentration and K_P the Stern-Volmer constant of the prompt fluorescence. Employing the Smoluchowski equation, the following relation between the Stern-Volmer constant and the diffusion length can be derived[23]:

$$L = \sqrt{\frac{6K}{4\pi R}}, \tag{7}$$

where R is the interaction radius and τ_0 the unquenched exciton lifetime. Here the assumption is made that once an exciton comes within the interaction radius of the quencher, it is immediately (with 100 % probability) quenched. To analyse the Stern-Volmer plot, we first determine the interaction radius of 1.2 nm, by using the static quenching of the excitons as further described in the supporting information[22]. With respect to the estimation of the interaction radius, we note that this is an approximation, as the interaction radius actually is slightly dependent on rate of singlet transfer. However, as we will see, this small uncertainty in interaction radius does not prohibit the extraction of meaningful diffusion lengths, and makes very little difference when the rate of transfer to the quencher is very high. In terms of guiding experiments, this indicates that the use of a strong charge-transfer quencher where electron transfer rates can be extremely fast (such as a fullerene derivative[34]) is sufficient to allow the extraction of valid diffusion lengths with this approach.

In order to extract the triplet diffusion length, a Stern-Volmer plot based on the delayed fluorescence can be used. However, in order to do this, the 'raw' data on the quenching of the delayed fluorescence must be slightly processed as it is influenced by: 1) the amount of quenching of the prompt fluorescence; 2) the motion of singlet

excitons regenerated after one (or more) cycle(s) through the triplet state; and 3) the triplet motion itself (considering all the cycles through the triplet state).

In Fig. 4 (a), the Stern-Volmer plot based on the raw quenching of the delayed fluorescence is shown. A clear difference in the quenching behaviour and a monotone dependence on the triplet diffusion length is observed. The figure further highlights that the raw delayed Stern-Volmer plots do not follow straight lines. The curvature is the most pronounced with the higher triplet diffusion lengths, but we note that the lines are not straight even in the case without triplet motion. There are two distinct reasons for this behaviour that will be discussed in the following. Firstly, the amount of delayed fluorescence is also directly affected by the quenching of the prompt fluorescence. The more excitons lost already during the prompt lifetime, the fewer that ever make it into the delayed time window. This makes it necessary to apply the following correction. The amount of delayed fluorescence as a function of acceptor concentration is reduced by a factor P/P_0 which is equal to one minus the quenching efficiency of the prompt fluorescence. Therefore, the D_0 becomes a function of acceptor concentration in the delayed Stern-Volmer plot and the equation must first be corrected to:

$$K_{\mathrm{D}}([Q]) = \frac{P}{P_0} \cdot \frac{D_0}{D} - 1, \tag{8}$$

with the delayed Stern-Volmer constant K_{D}. In Fig. 4 (b) the so-corrected Stern-Volmer plot is shown. Now, each data set corresponding to a certain triplet diffusion length is close to a straight line. But, one sees that even in the absence of triplet motion this 'line' has a non-zero slope. This is due to the recreation of singlets and their diffusion within the delayed time range. As a side note, we emphasize that at this point straight lines may not be obtained, especially for high acceptor concentrations, for a reason further elaborated below. A second note in this regard, is that the quenching rate of singlet states for nearest neighbor positions should be high in comparison to k_{ISC} (as it is in our simulations), otherwise triplets could be formed next to a quencher and a 'static' quenching component added to the delayed Stern-Volmer plot. This would also introduce a curvature to the delayed Stern-Volmer plot, but should be possible to avoid in real experiments as it is in our simulations by using a strong quencher.

The contribution of singlets to the quenching of the delayed fluorescence can be subtracted out using $n\phi_{\mathrm{RISC}}K_{\mathrm{P}}[Q]$, since the influence of singlet and triplet diffusion on K_{D} based on Eq. 5 and 7 is given by:

$$K_{\mathrm{D}}[Q] = (\underbrace{4\pi R_s D_{\mathrm{s}} \tau_{\mathrm{s}}}_{=K_{\mathrm{P}}} n\phi_{\mathrm{RISC}} + \underbrace{4\pi R_t D_{\mathrm{t}} \tau_{\mathrm{t}} n}_{=K_{\mathrm{t}}})[Q]. \tag{9}$$

The delayed quenching due only to triplet motion is shown in Fig. 4 (c). This is corrected for both the prompt quenching and the portion of the delayed quenching due to singlet motion. Theoretically, the slope should be zero in the case that the triplet diffusion length is zero. However, we see that in the case of zero triplet diffusion length there is a small negative slope. This artefact is the result of two effects, both of which should also be present in experimental data. Firstly, singlet states regenerated during the delayed lifetime actually have a lower probability to reach a quencher than a singlet generated by photoexcitation. This is because the regenerated singlets are not created with a spatially-uniform density as those created by absorption events, but rather at positions which are

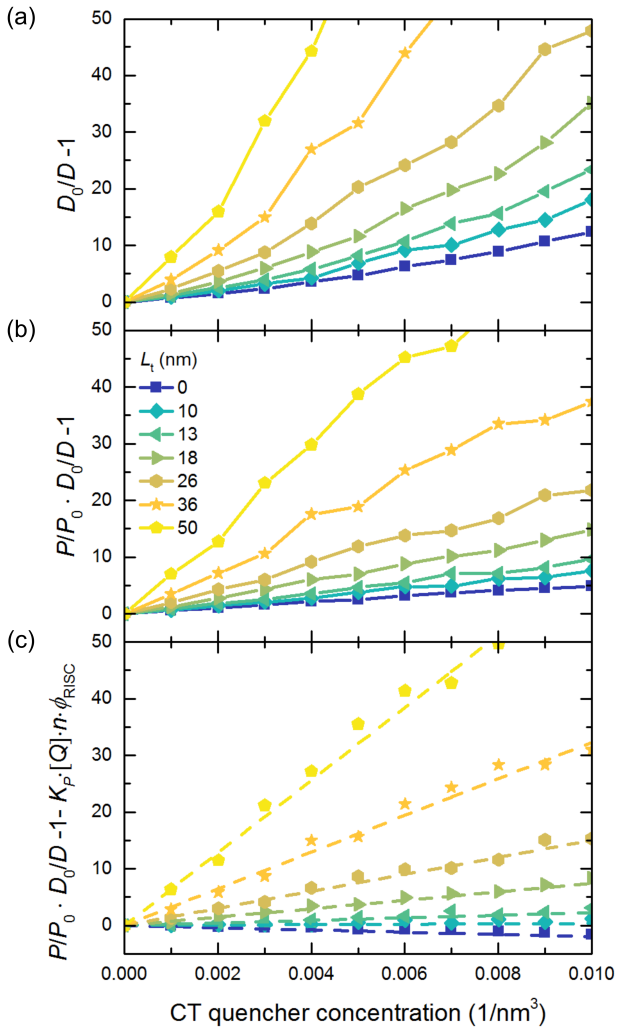

FIG. 4. Stern-Volmer plot based on the delayed PLQY. Here, P_0 and D_0 are the unquenched prompt and delayed and P and D the quenched prompt and delayed PL intensities, respectively. (a) shows the Stern-Volmer plot based on the raw delayed fluorescence data. In plot (b) D_0 is corrected for the quenching of the prompt fluorescence leading to a reduced ISC efficiency. In graph (c) the Stern-Volmer plot has been further corrected for quenching due to singlet motion in order to yield a slope directly proportional to L_t^2. In plot (a) and (b) the lines are guides for the eye, while in plot (c) linear fits are shown.

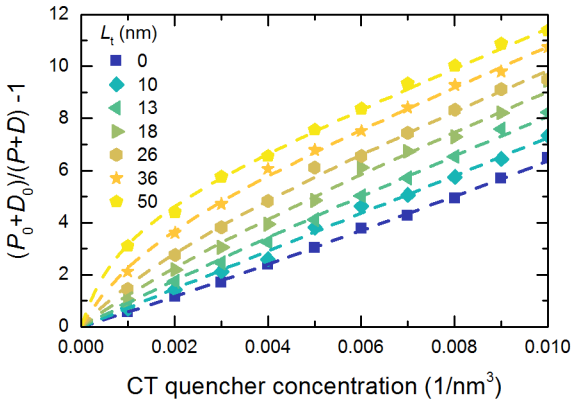

FIG. 5. Stern-Volmer plot based on the steady state PLQY. The dashed lines correspond to fits based on Eq. 9 and Eq. 10, where K_t was the only free parameter.

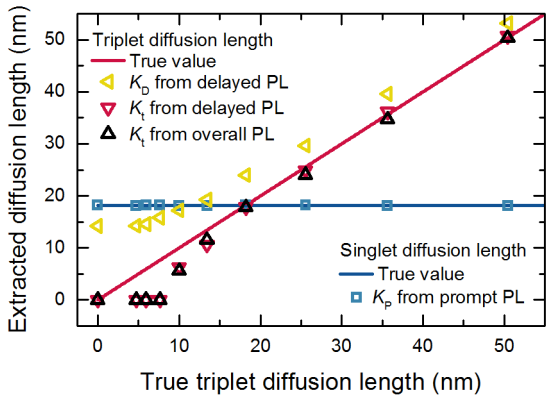

FIG. 6. Extracted diffusion length of singlet and triplet excitons by Stern-Volmer plots based on prompt, delayed and overall fluorescence. The diffusion length of the singlets was determined by using the data in Fig. 3, For the triplets the diffusion length has been extracted by using the second and bottom plot of Fig. 4 (yellow and red triangles, respectively) as well as by using Eq. 5 together with the data in Fig. 5 (black triangles).

in average further away from the next quencher (due to the quenching within the prompt lifetime). Secondly, the singlet motion is quite likely sub-diffusive, i.e. the mean square displacement increases slightly sublinearly with time. At low TADF concentrations, the sub-diffusion can be caused by the limited size of the percolation network in which the excited-state can move. At 80 % matrix concentration the diffusion process is not strictly governed by Fick's second Law, but is sub-diffusive with $\alpha = 0.98$. This effect is further discussed in the supporting information and would be more severe for smaller FRET radii and lower TADF concentrations[22]. In real experiments, the energetic disorder is also likely to contribute to a slowing of the excited-state motion with time. Irrespective of the cause of the negative slope, we will see in the following that this prevents the accurate estimation of triplet diffusion lengths when the triplet diffusion length is less than roughly half of the singlet diffusion length.

As an aside, we note that instead of analysing the Stern-Volmer plots for the prompt and delayed fluorescence separately, it is also possible to analyse the Stern-Volmer plot obtained for the quenching of the total luminescence. This is of course very easily experimentally accessible, as it requires only the steady-state PL to be measured. Eq. 6 and 8 can be solved for P and D, respectively. These values can be inserted into $y([Q]) = (D_0 + P_0)/(D + P) - 1$, to yield a fit function for the Stern-Volmer plot of the total (steady-state) luminescence quenching:

$$y_1([Q]) = \frac{(D_0 + P_0) \cdot (K_D[Q] + 1) \cdot (K_P[Q] + 1)}{D_0 + P_0 \cdot (K_D[Q] + 1)} - 1. \tag{10}$$

It is now possible to insert Eq. 9 in Eq. 10 and fit to the Stern-Volmer plots based on the overall fluorescence with K_t being the only free parameter, while all other parameters can be kept constant and determined by separate experiments. In Fig. 5 the corresponding fits are shown. The extracted K_t lead to triplet diffusion lengths that are identical to the values extracted from the delayed fluorescence.

In Fig. 6 all extracted diffusion length are shown and compared to the true values, which are determined by tracking the mean square displacement of the simulated excitons. For the singlet diffusion length, a very good agreement, with deviations well below 5 %, can be achieved by analysing the prompt Stern-Volmer plot. In case of the triplet diffusion length, good results can be obtained if the diffusion length is bigger than about 50 % of the singlet diffusion length. In this regime, the deviation between the real and the extracted values are below 10 %. For $L_t << L_s$ the correction of singlet motion in the delayed Stern-Volmer plot leads to slopes (K_D) close to zero and small measurement errors of prompt and delayed fluorescence will therefore have a big impact on the determined diffusion length. In our case the slopes are negative for triplet diffusion length smaller 10 nm, which would lead to non-physical (complex) results of the triplet diffusion length. Therefore, we conclude that as long as the triplet diffusion length is larger than roughly half of the singlet diffusion lengths, both quantities can be obtained with good accuracy by appropriate analysis of the luminescence quenching in the presence of a strong electron acceptor.

B. Stern-Volmer analysis based on triplet-only quenchers

In this section, we investigate whether a more accurate estimation of the triplet diffusion length can be obtained in the case of small triplet diffusion lengths,

when triplet-only quenchers are used rather than charge-transfer quenchers. Rather than quenching both singlets and triplets (like charge-transfer quenchers), the triplet-only quenchers do not affect the singlet population and quench only the triplets. Therefore, the prompt fluorescence is not quenched at all, but the delayed fluorescence is. As triplet only quenchers organic small molecules can be employed with the singlet level above, and triplet level below the ones of the TADF molecule (compare Fig. 2), in case of 4CzBN anthracene would be a good candidate.

The Stern-Volmer plot for the quenching of the delayed fluorescence for a triplet-only quencher is shown in Fig. 4. With the triplet-only quenchers, there is a slight positive slope to the Stern-Volmer plot even when the triplet diffusion length is zero. In this case, this is due to the motion during regenerated singlet lifetimes. Motion during a phase in the singlet state can cause a triplet to be reformed near enough to a triplet quencher that it can be quenched as soon as the triplet is reformed. This leads to a constant overestimation of the triplet diffusion length (in our case by about 3 nm). Therefore, even turning to triplet-only quenchers, a trivial determination of small triplet diffusion lengths is not possible.

However, in the following we suggest two different methods to find and subtract this offset, in order to allow the accurate determination of a small triplet diffusion length.

A first strategy relies on the different distance dependence of the transfer rates of singlet and triplet states. When the TADF molecules are dilute in the matrix (i.e. less than >5 %) the triplet state becomes nearly immobile, while the mobility of the singlet state is less affected. This is especially true for the so far problematic cases of small triplet and long singlet diffusion lengths. Thus, the contribution of the quenching due to singlet motion can be established in a highly-diluted sample and then be subtracted from the total quenching in the sample with a higher TADF concentration. This leaves only the contribution to the quenching due to triplet motion and is illustrated in Fig. 9. Here, the green triangles represent the extracted diffusion length after subtraction of the quenching of a simulation with 98 % to 99 % matrix molecules. It can be seen that the extracted triplet diffusion lengths are then correct, even for low triplet mobility.

A second strategy would be to first accurately determine the singlet diffusion length (i.e. by using the prompt quenching of an charge transfer acceptor). Then the offset can be determined by a MC simulation using the given singlet diffusion length and a triplet diffusion length of zero. Once this offset is calculated, it can be subtracted from the experimentally-determined value.

Analogous to the previous section, it is not necessary to time-resolve the emission for the whole quencher concentration series. Once the unquenched prompt and delayed emission, P_0 and D_0, are known, then the Stern-Volmer plot for the total quenching (Fig. 8) can be fit by Eq. 11 and values for the diffusion length are extracted that are identical to those based on the analysis of only the delayed emission.

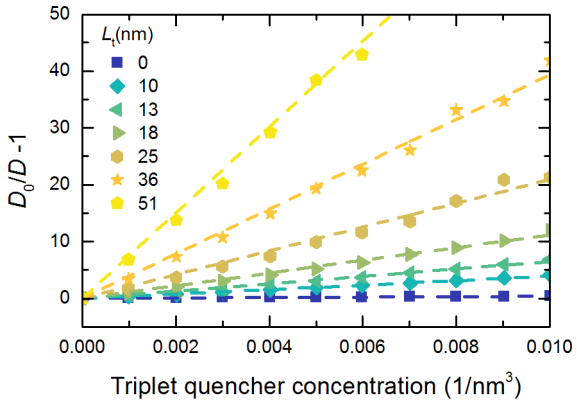

FIG. 7. Stern-Volmer plot based on the delayed PL quenching by a triplet-only quencher. The dashed lines correspond to linear fits used for the extraction of K_t^*.

$$y_2([Q]) = \frac{D_0 \cdot K_t^*[Q]}{D_0 + P_0 \cdot (K_t^*[Q] + 1)}. \tag{11}$$

Thus, by using triplet-only quenchers it should be possible to determine the triplet diffusion length, even when the triplet diffusion length is low. However, to do this one must first establish the singlet diffusion length. Therefore, we suggest using a strong charge-transfer acceptor (such as PCBM) in the first instance to determine the singlet diffusion length, and the triplet diffusion length in cases where the triplet diffusion length is equal or longer than that of the singlet. If the triplet diffusion length is short compared to that of the singlet, analysis with a triplet-only quencher could be of value. As discussed in the next section, the information about whether the triplet diffusion is poor compared to the singlet (certainly obtainable from the charge-transfer acceptor data) is already an interesting finding.

IV. IMPLICATIONS FOR HYPERFLUORESCENT DEVICES

Finally, we briefly consider (with MC simulations) how singlet and triplet diffusion affect the efficiency of hyperfluorescence. We consider the efficiency of transfer to a fluorescent emitter of excitons created on TADF molecules (with 75 % probability to be in the triplet state and 25 % probability to be in the singlet state to mimic electrical excitation). As the concentration of fluorescent acceptors must be kept low, most excitons created on the TADF will have to diffuse between TADF molecules in order to reach a fluorescent acceptor. Once a fluorescent acceptor is neared, the exciton can transfer by FRET if it is in the singlet state, or by Dexter transfer if it is in the triplet state. The former process is desired, and

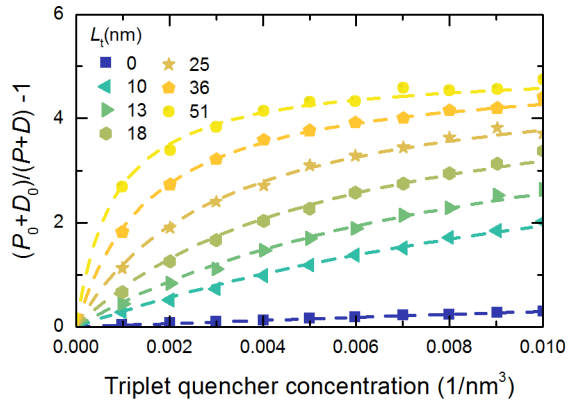

FIG. 8. Stern-Volmer plot based on the steady state PL quenching by a a triplet-only quencher. The dashed lines correspond to fits based on Eq. 11, where K_t^* was the only free parameter.

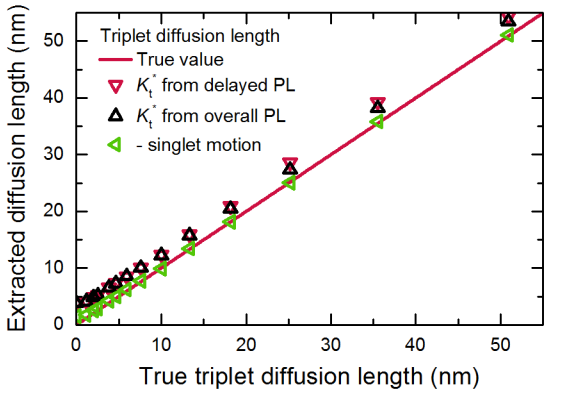

FIG. 9. Extracted diffusion length of triplet excitons by Stern-Volmer plots based on delayed and overall fluorescence.

results in an emissive singlet state on the fluorescent acceptor. The latter process is undesired, and leads to a terminal loss mechanism in the creation of a triplet state on the fluorescent acceptor. Naturally, the range of the FRET transfer is longer than that of the Dexter transfer. Fluorescent acceptors encased in a shielding sheath of inert side-chains to keep TADF molecules far enough away to selectively suppress the Dexter transfer may possibly be developed, however current generations of fluorescent acceptors lack this protection.

This raises the question, is triplet transport in the TADF molecules desirable? On the one hand, the improved diffusion could help excitons reach the fluorescent acceptor molecules. On the other hand it makes it more likely for the fluorescent acceptor to be neared when the exciton is in the triplet state, leading to terminal loss due to Dexter transfer to the acceptor.

In Fig. 10, the efficiency with which TADF excitons are harvested onto the singlet state of the fluorescent acceptor is shown. The y-axis represents the fraction of the total injected excitons that end up in the singlet state of the fluorescent acceptor. We simulate both unprotected and sterically protected fluorescent acceptors (those that allow/suppress Dexter transfer from nearby TADF molecules), and the variety of different triplet triplet diffusion lengths for the TADF molecule. For this simulation two new parameters in comparison to the simulations in Section III need to be introduced, namely the Förster radius between TADF and acceptor molecules (set to 3.3 nm) and the radius of the protecting shell surrounding the acceptors (set to 1.75 nm).

The best performance is achieved by the sterically-protected emitters, with 90 % of the excitons created on the TADF molecules feeding into the singlet of fluorescent acceptor at acceptor concentrations of around 5 %. Interestingly, for the unprotected molecules, triplet transport has a strongly deleterious effect on the harvesting efficiency. When the triplet diffusion length is comparable to the singlet diffusion length, only 20 % of the initial TADF excitons can be usefully harvested by the fluorescent emitter. However, if triplet transport between the TADF molecules can be suppressed, then 80 % harvesting can be achieved. Interestingly, this work reveals that there are two pathways towards reaching high efficiency hyperfluorescence. The first is to suppress triplet transfer to the fluorescent acceptors by developing appropriate steric protection. However, a second pathway, which is nearly as efficient, is to suppress the motion of triplets between TADF molecules. Given that triplet transfer requires the concurrent overlap of both HOMOs and LUMOs between two adjacent molecules, and given that the HOMOs and LUMOs of TADF molecules can be quite spatially separated, it is possible that it may not be too challenging to develop TADF molecules with low triplet diffusion lengths. Indeed, for some existing TADF materials it is likely that although the overlap of one frontier orbital between adjacent molecules is good, the overlap for the other frontier orbital is poor. This would mean some existing TADF molecules may already have limited triplet mobility, making them of special interest for hyperfluorescence applications.

V. CONCLUSIONS

Using simple MC simulations, we have examined how singlet and triplet diffusion lengths for TADF molecules can be determined from concentration-dependent quenching experiments. Our results suggest that the singlet and triplet diffusion lengths can be independently and accurately determined using charge-transfer quenchers as long as the triplet diffusion length is at least half of the singlet diffusion lengths. For shorter triplet diffusion lengths, moving to triplet-only quenchers may be sufficient to allow accurate determination. Finally, we suggest that the restriction of triplet motion is actually quite appealing for enabling efficient hyperflu-

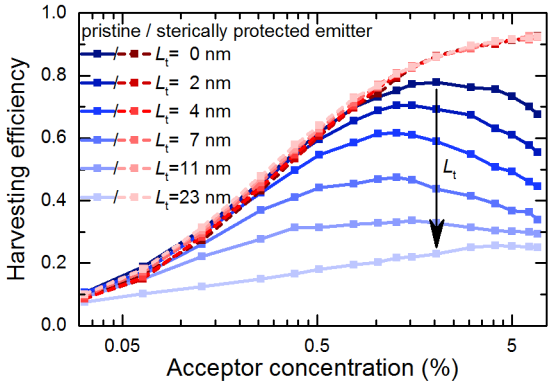

FIG. 10. Singlet harvesting efficiency of the emitter as a function of acceptor concentration relative to the donor concentration. Red data points correspond to sterically protected emitters, to allow only singlet states to transfer to the emitter via a long range FRET hop, while blue data points correspond to unprotected emitters. In both cases a set of different triplet diffusion length is shown, while the singlet diffusion length is kept constant at 18.1 nm.

orescence in OLED devices in the absence of specially-designed FRET acceptors that use steric protection to hinder their acceptance of triplet states. Therefore, we suggest that TADF molecules should be sought in which the triplet diffusion length is negligible compared with the singlet diffusion length. Experimentally, this could be established with the analysis we show of the charge-transfer quenching of the prompt and delayed fluorescence. Namely, a zero slope (or even better negative) on the modified Stern-Volmer plot of the delayed fluorescence is desirable as it indicates that the triplet diffusion length is negligible with respect to that of the singlet. In summary, these results both motivate and aid the further experimental investigation of the interesting exciton transport properties of TADF materials.

VI. ACKNOWLEDGMENTS

This work was financially supported by the German Research Foundation (DFG) through SFB 1176 (project A4). M.J. acknowledges support from KSOP graduate school.

* ian.howard@kit.edu

[1] M. A. Baldo, D. F. O'Brien, M. E. Thompson, and S. R. Forrest, Phys. Rev. B **60**, 14422 (1999).
[2] C. Adachi, M. A. Baldo, M. E. Thompson, and S. R. Forrest, Journal of Applied Physics **90**, 5048 (2001).
[3] Y. Kawamura, K. Goushi, J. Brooks, J. J. Brown, H. Sasabe, and C. Adachi, Applied Physics Letters **86**, 071104 (2005).
[4] W. Song and J. Y. Lee, Advanced Optical Materials **5**, 1600901 (2017).
[5] S. Kim, H. J. Bae, S. Park, W. Kim, J. Kim, J. S. Kim, Y. Jung, S. Sul, S.-G. Ihn, C. Noh, S. Kim, and Y. You, Nature Communications **9**, 1211 (2018).
[6] K. Goushi, R. Kwong, J. J. Brown, H. Sasabe, and C. Adachi, Journal of Applied Physics **95**, 7798 (2004).
[7] T. Hosokai, H. Matsuzaki, H. Nakanotani, K. Tokumaru, T. Tsutsui, A. Furube, K. Nasu, H. Nomura, M. Yahiro, and C. Adachi, Science Advances **3** (2017).
[8] Q. Zhang, B. Li, S. Huang, H. Nomura, H. Tanaka, and C. Adachi, Nature Photonics **8**, 326 EP (2014), article.
[9] Y. Tao, K. Yuan, T. Chen, P. Xu, H. Li, R. Chen, C. Zheng, L. Zhang, and W. Huang, Advanced Materials **26**, 7931 (2014).
[10] Q. Zhang, J. Li, K. Shizu, S. Huang, S. Hirata, H. Miyazaki, and C. Adachi, Journal of the American Chemical Society **134**, 14706 (2012).
[11] F. B. Dias, K. N. Bourdakos, V. Jankus, K. C. Moss, K. T. Kamtekar, V. Bhalla, J. Santos, M. R. Bryce, and A. P. Monkman, Advanced Materials **25**, 3707 (2013).
[12] M. Mamada, K. Inada, T. Komino, W. J. Potscavage, H. Nakanotani, and C. Adachi, ACS Central Science **3**, 769 (2017).
[13] C.-Y. Chan, L.-S. Cui, J. U. Kim, H. Nakanotani, and C. Adachi, Advanced Functional Materials **28**, 1706023 (2018).
[14] M. A. Baldo, D. F. O'Brien, Y. You, A. Shoustikov, S. Sibley, M. E. Thompson, and S. R. Forrest, Nature **395**, 151 (1998).
[15] S. M. Menke and R. J. Holmes, The Journal of Physical Chemistry C **120**, 8502 (2016).
[16] N. van der Kaap and L. Koster, Journal of Computational Physics **307**, 321 (2016).
[17] C. Groves, Energy Environ. Sci. **6**, 3202 (2013).
[18] M. Scheidler, U. Lemmer, R. Kersting, S. Karg, W. Riess, B. Cleve, R. F. Mahrt, H. Kurz, H. Bässler, E. O. Göbel, and P. Thomas, Phys. Rev. B **54**, 5536 (1996).
[19] T. Fŏrster, Discuss. Faraday Soc. **27**, 7 (1959).
[20] D. L. Dexter, The Journal of Chemical Physics **21**, 836 (1953).
[21] D. T. Gillespie, Journal of Computational Physics **22**, 403 (1976).
[22] See Supplemental Material at insert URL for more information regarding the verification of the simulation, the simulated photoluminescence quantum yield data, the impact of TADF/Matrix ratio on the diffusion process, the Stern-Volmer plots for simulations with triplet diffusion lengths below 10 nanometer and the estimation of quenching due to singlet motion when using a triplet-only quencher.
[23] J. R. Lakowicz, *Principles of Fluorescence Spectroscopy* (Springer, 2011).
[24] A. Haugeneder, M. Neges, C. Kallinger, W. Spirkl, U. Lemmer, J. Feldmann, U. Scherf, E. Harth, A. Gügel, and K. Müllen, Phys. Rev. B **59**, 15346 (1999).
[25] J. Wang, D. Wang, D. Moses, and A. J. Heeger, Journal of Applied Polymer Science **82**, 2553 (2001).
[26] B. A. Gregg, J. Sprague, and M. W. Peterson, The Journal of Physical Chemistry B **101**, 5362 (1997).

[27] S. R. Scully and M. D. McGehee, Journal of Applied Physics **100**, 034907 (2006).
[28] W. A. Luhman and R. J. Holmes, Advanced Functional Materials **21**, 764 (2011).
[29] M. A. Stevens, C. Silva, D. M. Russell, and R. H. Friend, Phys. Rev. B **63**, 165213 (2001).
[30] A. Lewis, A. Ruseckas, O. Gaudin, G. Webster, P. Burn, and I. Samuel, Organic Electronics **7**, 452 (2006).
[31] M. Hasegawa, S. Enomoto, T. Hoshi, K. Igarashi, T. Yamazaki, Y. Nishimura, S. Speiser, and I. Yamazaki, The Journal of Physical Chemistry B **106**, 4925 (2002).
[32] R. R. Lunt, N. C. Giebink, A. A. Belak, J. B. Benziger, and S. R. Forrest, Journal of Applied Physics **105**, 053711 (2009).
[33] O. V. Mikhnenko, H. Azimi, M. Scharber, M. Morana, P. W. M. Blom, and M. A. Loi, Energy Environ. Sci. **5**, 6960 (2012).
[34] G. Grancini, D. Polli, D. Fazzi, J. Cabanillas-Gonzalez, G. Cerullo, and G. Lanzani, The Journal of Physical Chemistry Letters **2**, 1099 (2011).